Effect of Pore Size, Solvation, and Defectivity on the Perturbation of Adsorbates in MOFs: The Paradigmatic Mg_2(dobpdc) Case Study

Jenny G. Vitillo*‡† and Gabriele Ricchiardi†

† Department of Chemistry, NIS Centre and INSTM, University of Turin, via Quarello 15, I-10135 Torino, Italy

‡ Department of Chemistry, University of Minnesota, 207 Pleasant Street S.E., Minneapolis, Minnesota 55455-0431, United States

J. Phys. Chem. C, **2017**, *121* (41), pp 22762–22772

DOI: 10.1021/acs.jpcc.7b06252

Publication Date (Web): September 25, 2017 **(WITH 12 MONTHS EMBARGO)**

Effect of Pore Size, Solvation and Defectivity on the Perturbation of Adsorbates in MOFs: the Paradigmatic Mg_2(dobpdc) Case Study

Jenny G. Vitillo,[‡†] * *Gabriele Ricchiardi* [†]

[†]Department of Chemistry, NIS Centre and INSTM, University of Turin, via Quarello 15, I-10135 Torino, Italy.

[‡] Department of Chemistry, University of Minnesota, 207 Pleasant Street S.E., Minneapolis, MN 55455-0431.

ABSTRACT. Mg_2(dobpdc) (H_4-dobpdc = 4,4'-dihydroxy-(1,1'-biphenyl)-3,3'-dicarboxylic acid) is an attractive metal organic framework (MOFs), because of its unique performances in carbon dioxide capture when combined with aliphatic amines. We have adopted this material as a paradigmatic case for the study of the effect of pore size, availability of open metal sites and structural defectivity on the sorptive properties of MOFs, with the aim of enabling the design of better sorbents and better tools for their characterization. In this study the adsorption of CO_2, CO, and N_2 has been investigated by means of infrared spectroscopy and high quality periodic quantum mechanical B3LYP-D* calculations. Comparison with literature data on the isomorph MOF-74-Mg, characterized by the shorter dobdc linker, allowed to verify a small, although appreciable effect of the pore size on the perturbation of the adsorbates. Although is is generally observed that the interaction energy with adsorbates decreases with increasing pore size,

Mg_2(dobpdc) represent an exception in the IRMOF-74 family and its interaction energy with adsorbates is greater than that of the smaller pore member of the family. The origin of this counterintuitive behavior was found in the increase of the dispersion energy component and in the lower framework deformation. The other typical aspects that can influence the interaction with guest molecules were investigated: the presence of residual solvents competing for adsorption and structural damage. For what concerns solvation, the affinity for solvents with different polarity was tested. Selective capping of the main adsorption sites (Mg^{2+}) was achieved by preadsorbing CH_3OH on the open metal sites. IR spectroscopy of CO adsorption at 100 K revealed to be able to detect the presence of molecules pre-coordinated to Mg^{2+} and then to check the quality of activation procedures for MOFs with open Mg^{2+} sites. Because of Mg_2(dobpdc) air-sensitivity, a full IR characterization was also performed after damaging by exposure to a water saturated atmosphere. Surprisingly, in spite of the drastic structural collapse verified by nitrogen volumetry (decrease of 83% in the surface area), the effect of damaging on the infrared spectrum of the MOF was negligible. Similarly, the only change observed in the spectra of the probe molecules was a slight decrease in their intensity after damaging. This means that IR spectroscopy is not a reliable technique to evidence the degradation of this MOF, unlike what reported for other systems.

INTRODUCTION

Metal organic frameworks (MOFs) are a class of important materials in several application fields with potential direct repercussion on society.[1] They are characterized by a modular structure based on inorganic secondary building units (metal/metal oxide clusters) connected by organic linkers. The dimensionality and coordinative insaturation of the inorganic clusters and of the organic linkers direct the material framework structure, giving often rise to crystalline structures

characterized by large and permanent porosity.[2] The adsorption performances of these materials are more sensitive to the degree of solvation and to structural integrity than in other classes of materials. Nevertheless, systematic studies on solvated or defective materials are rare.[3-5] We have adopted this material as a paradigmatic case for the study of the effect of pore size, availability of open metal sites and structural defectivity on the sorptive properties of MOFs, with the aim of enabling the design of better sorbents and better tools for their characterization.

Mg_2(dopbdc) (H_4-dobpdc = 4,4'-dihydroxy-(1,1'-biphenyl)-3,3'-dicarboxylic acid) is a metal organic framework whose structure results from parallel MgO_5 rows arranged in an hexagonal "honeycomb" structure. The linkers connect the Mg^{2+} rows by means of their carboxy and hydroxy groups, thus forming the walls of the honeycomb. Since all of the oxygen atoms of the linker are involved, this results in rows of MgO_5 coordination polyhedra, leaving one coordinative insaturation on Mg^{2+}. Each dobpdc^{4-} linker is shared between two rows. The resulting structure is reported in part a of Figure 1. In the as-synthetized material the sixth coordination position around Mg^{2+} is occupied by a solvent molecule which can be easily removed upon thermal treatment. The vacancy left can then be occupied by a guest molecule with beneficial effects on gas and liquid uptakes and on the stability of guests/MOF composites. The presence of this vacancy is at the basis of the high performances of MOFs isomorphous to Mg_2(dobpdc) in gas storage[6-7] and separation[6,8] applications. Several uses of Mg_2(dobpdc) can be envisaged, such as the purification from CO, CO_2 and N_2 of hydrogen obtained by gasification of biomasses.[9] Among them, those relevant to Carbon Dioxide Capture and Sequestration processes (CCS) hold a particular interest.[10] It is not surprising that the isomorphous MOF-74-Mg (or Mg_2(dobdc) with H_4-dobdc = 2,5-dihydroxytereftalic acid; see Figure S14),[9] is considered the benchmark material among MOFs in CCS studies.[6,11] The possibility to bond guest species

directly on the metal site provides the high temperature stability of diamine/Mg_2(dobpdc) composites, among the most promising systems for CO_2 capture from air, where the main competiting adsorbates are N_2 and H_2O.[12-13]

In this study, adsorption of CO_2, CO and N_2 on Mg_2(dobpdc) was investigated with a method combining infrared spectroscopy and high quality periodic quantum mechanical calculations, providing spectroscopic, energetic and structural features. The state-of-the-art computational study on full periodic models, was computationally challenging because of the system size. We adopted the B3LYP-D* level of theory, which combines the efficiency of the density functional method (DFT) B3LYP with the Grimme's scheme to include the long range dispersion interactions.[14-15] This high level of computational effort was needed in order to allow a direct comparison with the experiments and a precise assignment of the vibrations. The results were compared with those reported in a similar study on MOF-74-Mg,[9] an isomorphous material to Mg_2(dobpdc), presenting the same Mg^{2+} sites but a smaller pore dimension (15 versus 22 Å). This comparison allowed to study the effect of the pore structure on gas adsorption features. This is an interesting example of how the structural modularity of MOFs allows to conduct fundamental studies on the separate contributions of the different components of a material (linker, metal node) to a phenomenon,[7,16-17] both from a theoretical and experimental point of view.[7, 10] The correlation among structural, vibrational and energetic observables was investigated.

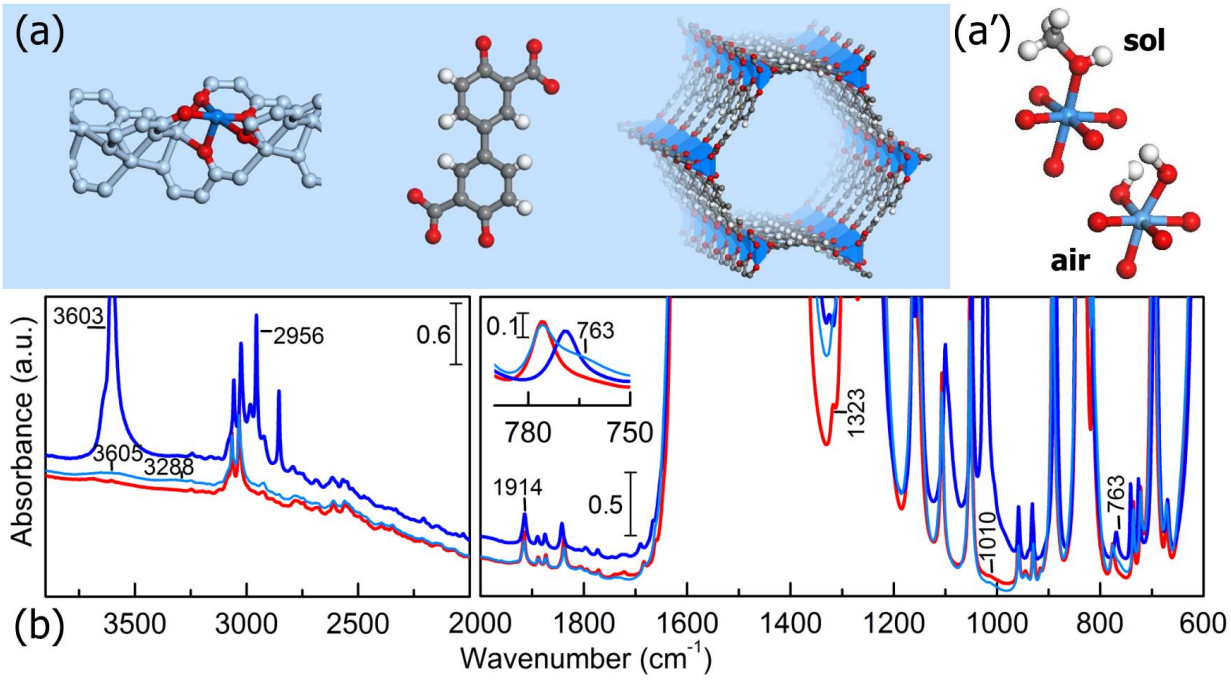

Figure 1. (a) From left to right: inorganic node, organic linker and the Mg_2(dobpdc)–*act* structure, as optimized at the B3-LYP-D*/TZVp level. The C atoms are reported in gray, H atoms in white, O in red, Mg in dark cyan. (a') A description of the first coordination sphere around Mg^{2+} site in Mg_2(dobpdc)–*sol* (as obtained at the B3LYP-D*/TZVp level, results not shown) and Mg_2(dobpdc)–*air* samples (as in Ref. 3) is also illustrated. (b) FTIR spectra of Mg_2(dobpdc)–*act* (red curve), Mg_2(dobpdc)–*sol* (blue curve) and Mg_2(dobpdc)–*air* (light blue curve) recorded in vacuum at RT. The three samples were activated before spectrum recording at 180, 25 and 250°C, respectively, for 15 h in dynamic vacuum.

Similar analyses have already been reported for other MOFs, [7, 10], and specifically for the larger members of the IRMOF-74 family. We report for the first time an anomalous pore-size dependence of adsorption properties for Mg_2(dobpdc), which is the second smaller member of the family. In the process of analyzing gas adsorption in Mg_2(dobpdc), we have also studied the

solvated material and the effect of the typical structural damage caused by hydrolysis in moist air, which is very typical of most MOFs. Spectroscopic studies on gas adsorption in MOFs are rarely dealing with not activated[4] or damaged materials.[5] Nevertheless, such studies would represent a useful benchmark to easily identify the effectiveness of activation protocols and the materials' robustness to handling and activation. They would also be useful for evaluating the impact of poisoning and damaging on the way the material perturbs an adsorbate. These points are particularly important for MOFs with open metal sites and for air sensitive MOFs, respectively.

Therefore, in the present work the changes in the infrared spectra of CO_2, CO and N_2 upon Mg_2(dobpdc) degradation or complete poisoning of the Mg^{2+} sites have been evaluated. For what concerns this last point, several solvents of increasing polarity were tested (toluene, CH_2Cl_2, CH_3OH, H_2O) in order to identify a candidate capping agent able to bind irreversibly only the Mg^{2+} sites at room temperature, without causing MOF degradation. In fact, the knowledge about the interaction of solvents with highly porous materials like MOFs is relevant for designing synthetic paths in post-synthesis modification,[12] formulation and shaping.[18] Besides qualitative evaluation by means of IR spectroscopy, the repercussions of material degradation and of the complete poisoning of the Mg^{2+} sites on the gas uptake were evaluated quantitatively for CO_2 and N_2 by means of comparative volumetric measurements at RT and 77 K, respectively.

MATERIALS AND METHODS

Materials. *Mg_2(dobpdc)–act*: Mg_2(dobpdc) was synthetized as reported previously.[7] It was then washed three times in dimethylformamide followed by three times in methanol. The sample was then degassed at 180°C for 15 h in dynamic vacuum ($p < 5 \cdot 10^{-4}$ mbar) before all the measurements.

Mg_2(dobpdc)–sol: Mg_2(dobpdc)–*act* was exposed to a saturated methanol vapor atmosphere at 25°C for 1 h and then degassed at RT for 15 h in dynamic vacuum ($p < 5 \cdot 10^{-4}$ mbar).

Mg_2(dobpdc)–air: Mg_2(dobpdc)–*act* samples after full characterization were exposed to a pure water vapor atmosphere at saturation pressure at 25°C for 24 h and then degassed for 1 h at RT followed by thermal treatment at 250°C for 15 h in dynamic vacuum ($p < 5 \cdot 10^{-4}$ mbar). The same pellet was used for the preparation and measurement of the *–act*, *-sol* and *–air* samples, This allowed a direct comparison of the intensity of the adsorbed probes in the IR study.

FTIR spectroscopy in transmission. In situ FTIR spectra in transmission mode (2 cm^{-1} resolution, average of 64 scans) were collected on a Bruker Vertex70 spectrophotometer equipped with a mercury cadmium telluride detector. The samples were measured in the form of self-supporting pellets placed in a cell allowing to work in controlled atmosphere The pressure in the preparation of the pellets was below 1.8 MPa.

Volumetric measurements. Nitrogen and carbon dioxide adsorption isotherms were measured on a commercial volumetric apparatus (Micromeritics ASAP2020). During the N_2 measurements, the temperature was maintained constant at 77 K by means of a liquid nitrogen bath, whereas for the CO_2 isotherms a circulating liquid bath was adopted (Julabo, F25-HE). The specific surface area was obtained by using the Langmuir and B.E.T. [19-20] methods in the standard pressure range ($0.05 < p/p_0 < 0.20$). All the reported quantities are affected by an error of 10%.

Periodic calculations. Density Functional theory (DFT) calculations have been performed using the CRYSTAL14 program[21] by means of the Becke's three-parameters hybrid exchange functional[22] supplemented with the Lee, Yang, and Parr's gradient-corrected correlation functional[23] and corrected with the scheme to include the long range dispersion interaction

proposed by Grimme[14] and slightly modified by Civalleri et al.[15] for the study of solids (hereafter B3LYP-D*). All-electron Gaussian type basis sets of triple-ζ valence quality were adopted for all the atoms as optimized in Ref. 9 to study the CO_2, CO and N_2 complexes with the isomorph MOF MOF-74-Mg and reported in Ref. 24 (TZVp for Mg and TZV for C, O, H). The Mg_2(dobpdc) cell used in the calculations has a hexagonal lattice with a space group $P3_221$ and contains three formula units ($Mg_6C_{42}H_{18}O_{18}$). The starting geometry for the empty MOF was obtained from the structure reported in Ref. 7 for the analogous Co_2(dobpdc). Lattice parameters and atom positions were fully optimized by keeping fixed the initial group symmetry. The cell parameters calculated with the inclusion of the D* terms are closer to their experimental values ($a = b$ = 21.7008(8) Å and c = 6.847 (1) Å).[5] The differences with respect to the calculated values 0.5/0.9% and 0.8/2% with and without the correction (see Section S2 of the SI). For the gas complexes, a loading of 1 gas molecule per Mg^{2+} was considered by maintaining the $P3_221$ symmetry. For the CO and N_2 complexes, the optimization with $P3_221$ symmetry ended up in a minimum geometry. On the contrary, the CO_2 complex was characterized by 5 imaginary frequencies. A scan along one imaginary mode was used to obtain a starting geometry for the CO_2 complex, characterized by a $P3_2$ symmetry. This structure is a minimum geometry and it will be used in the discussion if not otherwise specified.

For numerical integration of the exchange-correlation term, a (75 974) pruned grid was adopted.[21] The threshold conditions for convergence in self-consistent field (SCF) iterative procedure was set to 10^{-8} and 10^{-10} hartree for geometry and frequency calculations, respectively. The Pack−Monkhorst/Gilat shrinking factors for the reciprocal space were set to 3 and 3, corresponding to seven and seven points at which the Hamiltonian matrix was diagonalized. The accuracy of the integral calculations was increased by setting the tolerances to 7, 7, 7, 7, and 25.

To accelerate convergence in the SCF process, a modified Broyden's scheme,[25] following the method proposed by Johnson,[26] was adopted. The method was applied after 5 SCF iterations, with 50 % mixing of the Fock/Kohn–Sham (KS) matrices and the Johnson's parameter set to 0.05. The above computational parameters ensured full numerical convergence on all computed properties described herein.

Binding energies of the gas on the MOF have been corrected for the basis set superposition error (BSSE) by the *a posteriori* Lendvay and Mayer approach.[27] Vibrational frequencies at the Γ point and their IR intensities were calculated on the optimized geometries by means of a mass-weighed Hessian matrix, obtained by numerical differentiation of the analytical first derivatives.[28]

RESULTS

Vibrational characterization of the adsorbents. *Mg_2(dobpdc)–act.* Thermal desorption was investigated in order to locate the minimum temperature necessary for complete removal of solvents. The IR spectrum of Mg_2(dobpdc) recorded in transmission after degassing at 180°C for 15 h is reported as red curve in Figure 1b (Mg_2(dobpdc)–*act*). The complete removal of solvents (water and methanol, see Refs. [4,29] and below) is proved by the absence of any band in the 3700-3300 cm^{-1} region, confirming the efficacy of the activation procedure. Analogous spectra (not shown) were obtained after treatment at 200°C for 5 h, while degassing at temperatures lower than 180°C did not allow the complete removal of methanol. This result differs from what previously reported for MOF-74-Mg, which was completely activated already at 160°C for 15 h.[9] The absence of bands in the 3700-3300 cm^{-1} region suggested also the low defectivity of this sample,[5,29] as confirmed by XRD and nitrogen volumetry (a complete characterization of this sample is reported in Ref. 5). The absence of the dimethylformamide IR fingerprint (carbonyl

stretching at 1665 cm^{-1})[30] indicates its complete removal through the methanol exchange procedure performed at the end of the synthesis. The IR spectrum of Mg_2(dobpdc)–*act* was also recorded in attenuated total reflectance (ATR, see Figure S2) in order to locate the maxima of the intense framework IR bands. A list of the MOF IR bands and their assignment on the basis of the calculations is reported in Table S1. Briefly, the MOF spectrum is dominated by two pairs of bands situated at (i) 1616 and 1573 cm^{-1} due to benzene ring stretching vibrations and (ii) at 1467 and 1425 cm^{-1} due to the asymmetric and symmetric stretching frequency of the carboxylate groups. Two other intense signals are located at 1293 and 1239 cm^{-1} and are associated to C-O stretching of the alcoholate species in combination with C-C stretching of the phenyl rings accordingly to what previously reported for CPO-27-Ni.[31]

Mg_2(dobpdc)–sol and Mg_2(dobpdc)–air. The selective poisoning of Mg^{2+} was investigated by using solvents of increasing polarity: toluene, CH_2Cl_2, CH_3OH and H_2O. IR spectroscopy was used to follow the adsorption and desorption processes, to verify the coordination of the solvent molecules to the Mg^{2+} sites and to identify irreversibly adsorbed species.

The recorded spectra are reported in Figure S3-S7. In all cases, a vapor pressure higher than that sufficient to fully saturate the Mg^{2+} was dosed. As a common feature, solvent adsorption is always accompanied by a perturbation of all the MOFs modes. The family of bands at about 1900 cm^{-1} (assigned to overtones and combinations of frameworks modes) and the signals at 958, 929 and 776 cm^{-1} are the most sensitive to the adsorption of solvents, shifting and broadening significantly. Their shifts are listed in Table S2. The most important band shifts are observed in the case of toluene. Toluene (Figure S3) and CH_2Cl_2 (Figure S4) are adsorbed reversibly at the beam temperature (BT, estimated around 40-50°C). For the two most polar solvents CH_3OH (Figure S5) and H_2O (Figure S7), on the contrary, the solvent molecules in

interaction with the organic part of the MOF were fully removed at beam temperature, whereas adsorbates directly coordinated with Mg^{2+} necessitated higher desorption temperatures. For what concerns methanol, after prolonged degassing at beam temperature, an extra band with respect to the Mg_2(dobpdc)–*act* spectrum was still present in the 3700-3300 cm^{-1} region (see blue curve in Figure 1b). This band, located at 3603 cm^{-1}, is associated to methanol molecules coordinated to the open metal sites. This sample is referred in the following as Mg_2(dobpdc)–*sol*. After degassing at 180°C for 15 h, the spectrum was restored to that recorded for the pristine Mg_2(dobpdc)–*act*. Moreover, the surface area measured was identical to that of -*act* indicating that methanol does not damage the MOF structure. From all these evidences, methanol emerges as a good capping agent and was then used for this purpose in the gas adsorption study.

Water, on the contrary, did not show to be a good choice for this aim. In fact, after contact with a water vapor pressure of 20 mbar (saturation pressure at 20°C) and prolonged degassing at beam temperature, the spectrum showed the presence of two additional bands at 3687 and 3600 cm^{-1} associated respectively to the asymmetric and symmetric stretching of water molecules directly coordinated to Mg^{2+} (see light blue curve in the lowest part of Figure S7). A similar assignment was made previously for MOF-74-Mg by combining IR spectroscopic data and DFT calculations.[3-4] The irreversibility of water molecules adsorbed on Mg^{2+} was expected on the basis of the large adsorption enthalpy (-73-80 kJ mol^{-1}) reported for MOF-74-Mg.[4] Bands at a slightly lower frequency (larger shift) were reported for the interaction of water with MOF-74-Mg[4] (see Table 1) suggesting a lower affinity of Mg_2(dobpdc) towards water because of its larger pore size. A third broad band centered at about 3350 cm^{-1}, associated to –OH species involved in hydrogen bonding,[32] remained present in the spectrum also after prolonged outgassing at beam temperature. These hydroxy groups can be associated to persisting water molecules belonging to

a second coordination sphere of Mg^{2+}. Nevertheless, it is important to stress that during water adsorption and desorption hysteresis is observed (Figure S7): the 3350 cm^{-1} band observed during water desorption corresponds to two broad bands observed in adsorption, situated at 3352 and 3231 cm^{-1} and associated to hydrogen bonded water molecules. Similar bands were reported at 3380 and 3223 cm^{-1} in MOF-74-Mg.[4] Such a change in the spectral sequence suggests a material modification in time. The band at 3350 cm^{-1} is more likely associated to couples of –OH formed because of the partial hydrolysis of the material and to water molecules involved in hydrogen bonding with these species.[3,5] The degradation of the sample after exposure to a saturated water atmosphere has been proven in a previous study.[5] After subsequent activation of the MOF at 200°C (see Figure S8), the spectrum of Mg_2(dobpdc)–*act* was not fully restored: three new broad signals with very low intensity appeared at 3605, 3288 cm^{-1} and 763 cm^{-1} (see light blue curve in Figure 1b). In particular, the signals at 3605 and 3288 cm^{-1} are not even clearly visible on thin pellet . These signals have been previously associated to defects in the material due to hydrolysis and in particular to the formation of vicinal Mg-OH and HO-C couples due to water splitting in the first step of the degradation process, then followed by pore blocking and structure collapse.[3,5] The hydroxyls groups created by hydrolysis apparently do not condense to the original structure upon water removal. In fact, although a decrease in the intensity of the –OH signals was observed upon increasing the treating temperature (Figure S8), for temperatures higher than 250°C, a contemporaneous decrease of the number of the available Mg^{2+} sites was observed (as quantitatively estimated comparing the intensity of the IR signal of adsorbed N_2) accompanied by a change in the sample color from whitish to yellowish. On this basis the optimal temperature for the activation of this sample was individuated to be 250°C,

although a full restoration of the open Mg^{2+} sites was not achieved (light blue curve in Figure 1b). This defective sample is indicated in the following as Mg_2(dobpdc)–*air*.

It is interesting to notice that when Mg_2(dobpdc)–*act* was exposed to a water vapor pressure lower than 0.5 mbar, the IR spectrum showed only the presence of the two bands at 3687 and 3600 cm^{-1} (light blue curve in Figure S8), attributed to water molecules directly coordinated to the Mg^{2+} sites, which are too far apart from each other to allow the formation of hydrogen bonds. For these low pressures, reactivation at 200°C allowed the recovery of the initial spectrum of the material, that is no material damage was evidenced. This suggests that MOF hydrolysis requires the presence of more than one water molecule per Mg^{2+} site to start. This result is in agreement with previous works on this topic.[3,5]

Besides the reversibility of the adsorption process, solvent polarity influenced also the time evolution of the adsorption process. In fact, for toluene and dichlorometane (that is for the solvents having the lowest polarity) the time evolution of the IR spectra after each vapor dosage was characterized by a parallel increase of the intensity of all the solvent bands until equilibration was reached. In the case of methanol, different behaviors were observed at different pressures. At pressures lower than 1 mbar, after each pressure step a slow evolution is observed. Initially, methanol prefers to interact with other methanol molecules through hydrogen bonding (band at 3309 cm^{-1}) instead to coordinate to the MOF (peak at 3603 cm^{-1}). Only in a second time, they slowly migrate on the Mg^{2+} sites. The process can be easily followed in time by means of IR spectroscopy, showing the decrease in the intensity of the 3309 cm^{-1} signal and the parallel increase of that located at 3603 cm^{-1} at each pressure pulse. In a qualitative description of the process, on the basis of the partial information obtained from the IR spectra, firstly the methanol molecules interact with the MOF walls preferentially through the methyl group leaving the -OH

free to interact by hydrogen bonding with other methanol molecules forming small aggregates likely outside the pores. The slow diffusion of aggregates in the MOF pores and their interaction with an open Mg^{2+} site would cause the transfer of one methanol molecule from methanol clusters to the metal sites. At equilibrium, all the methanol molecules are coordinated to a Mg^{2+} site. At pressures higher than 1 mbar (even in the case of the first pressure dosage), this first step is not observed and coordination to Mg^{2+} occurs from the beginning. For what concerns water, such a process was not observed likely because of the strong polar nature of this molecule and its higher interaction energy with the Mg^{2+} sites.

Table 1. Experimental vibrational stretching frequency (in cm^{-1}) of H_2O, CO_2, CO and N_2 adsorbed on MOF-74-Mg and Mg_2(dobpdc) materials as obtained at low coverage. The corresponding value for adsorption in silicalite, taken as a reference, is also reported.

	Silicalite	MOF-74-Mg[a]	MOF-74-Mg–*sol*[b]	Mg_2(dobpdc)–*act*	Mg_2(dobpdc)–*sol*	Mg_2(dobpdc)–*air*
CO_2 (ν_3)	2338[b]	2353	2343	2354	2344	2354
CO	2135[a]	2178	–	2182	2175/2152/ 2144	2182
N_2	2321[c]	2339	–	2341	-	2341
H_2O	3700-2700[d]	3663,3576	–	3687, 3600	–	–

[a]Ref. 9 for CO_2, CO and N_2. Ref. 4 for H_2O. [b]Ref. [33].[c]Raman signal at 240 K from Ref. 9. [d]Ref. [34]. [e]From Ref. 4; obtained on MOF-74-Mg after preadsorption of H_2O or NH_3.

CO_2 adsorption. Infrared spectra of CO_2 adsorbed on Mg_2(dobpdc)–*act*, Mg_2(dobpdc)–*sol* and Mg_2(dobpdc)–*air* at BT for increasing equilibrium pressures up to 44 mbar are reported in Figure

2 in the range interested by the CO_2 asymmetric stretching frequency ν_3 (2490-2210 cm^{-1}). The spectra in the whole region of acquisition (3800-600 cm^{-1}) are reported in Figure S10 along with zooms on the 3800-3540 cm^{-1} (CO_2 Fermi resonance) and 680-630 cm^{-1} regions (bending modes, ν_2).

For Mg_2(dobpdc)–*act*, at lower coverage, the first signals related to CO_2 are due to molecules directly coordinated to Mg^{2+} at 2354 and 2342 cm^{-1} (see part –*act* in Figure 2), in analogy with what has been reported for MOF-74-Mg, although at slightly higher wavenumbers.[9,35] These two bands have been associated to the ν_3 mode in the fundamental and in the excited vibrational ν_2 state after coordination of CO_2 to Mg^{2+}, respectively.[35] The band at 2288 cm^{-1} can be assigned to the same mode in $^{13}CO_2$. Their small shifts with respect to CO_2 in the gas phase (2349 and 2337 cm^{-1}) are due to the almost compensating effects of the electrostatic perturbation by a positive charge (blue shift) and the strong matrix effect (red shift) exerted by the microporous environment.[33,36] This means that in microporous materials, the frequency shifts of adsorbed molecules are underestimated if the gas phase frequency is taken as reference value. This should be considered when comparing with calculated properties. It is then common in the literature on the subject to adopt as reference value the frequency recorded in a low polarity microporous scaffold, like zeolite silicalite-1.[18,33,36-3933] For this reason, the value reported for adsorption in silicalite-1 is here used as reference value to calculate the experimental frequency shift for the three molecular probes used in this study (see Table 1 and Table 2). In the following only the ν_3 mode will be considered for CO_2 in the discussion.

At increasing CO_2 pressures, no new signal appears for CO_2 but an increase in the intensity of all the IR signals is observed. This indicates that in the conditions adopted, all CO_2 molecules are

interacting with Mg^{2+}. This qualitative conclusion is in agreement with volumetric measurements that confirm at 44 mbar an uptake significantly lower than the one corresponding to the saturation of all the Mg^{2+} sites (6 mol kg^{-1}, see Figure S9b).

For what concerns the calculations, they have been carried out considering a model where all the CO_2 are coordinated with a Mg^{2+} and vice versa, in order to maintain the symmetry of the model. The optimized structure is reported in Section S1. The calculated frequency shift ($\Delta\tilde{\nu}$) are reported in Table 2. Six IR–*act*ive modes are predicted in the CO_2 stretching range: $\Delta\tilde{\nu}$ = 0.5 (doubly degenerated), 6, 17 (doubly degenerated) and 18 cm^{-1}, each of them involving the contemporaneous stretching of six or four CO_2 molecules per unit cell. The CO_2 mode observed at 2342 cm^{-1} is then also due to the contribution of a mode with $\Delta\tilde{\nu}$ = 6 cm^{-1}. A slight modification of the MOF structure upon CO_2 adsorption was predicted by the calculations both at the long range (decrease of -1.3% of the cell volume) and at the short range (increase of 0.01 Å of the average Mg-O bond length). The decrease in the cell volume was observed in the calculations only for CO_2 adsorption, while CO and N_2 caused only a slight increase: ΔV = +0.2% and +0.1% for CO and N_2 respectively. Optimization in the same space group of the CO and N_2 complexes ($P3_221$) brought to no significant modification in the cell volume. So, if on one hand this difference with respect to the other gas complexes can be related to the different space group, on the other hand it can be easily explained by the stronger intermolecular interactions exerted by CO_2 molecules with respect to CO and N_2. Intermolecular interactions are well known to be particularly beneficial on CO_2 adsorption energy because of its large polarizability,[40] facilitating adsorbate self-assembling in the pores of the hosting material.[16] It is also well known that porous structures can shrink in the first step of the adsorption process in order to increase the interaction with and among the adsorbates.[41-42] Although the deformation

energy paid to decrease the cell volume is positive (0.9 kJ mol^{-1}), it is fully compensated by the increase in the dispersion energy going from 23.1 to 25.7 kJ mol^{-1} for the $P3_221$ and the $P3_2$ geometry, respectively.

The calculated Mg···O-C angle is 124°, unlike CO and N_2 that form almost linear complexes with the Mg site. A similar geometry was previously reported for MOF-74-Mg (∠Mg···O-C = 129°).[9] This peculiar geometry was explained by the strong quadrupolar nature of CO_2 and the possibility to maximize the interaction with the framework by involving both the Mg^{2+} and a vicinal O atom of the linker.

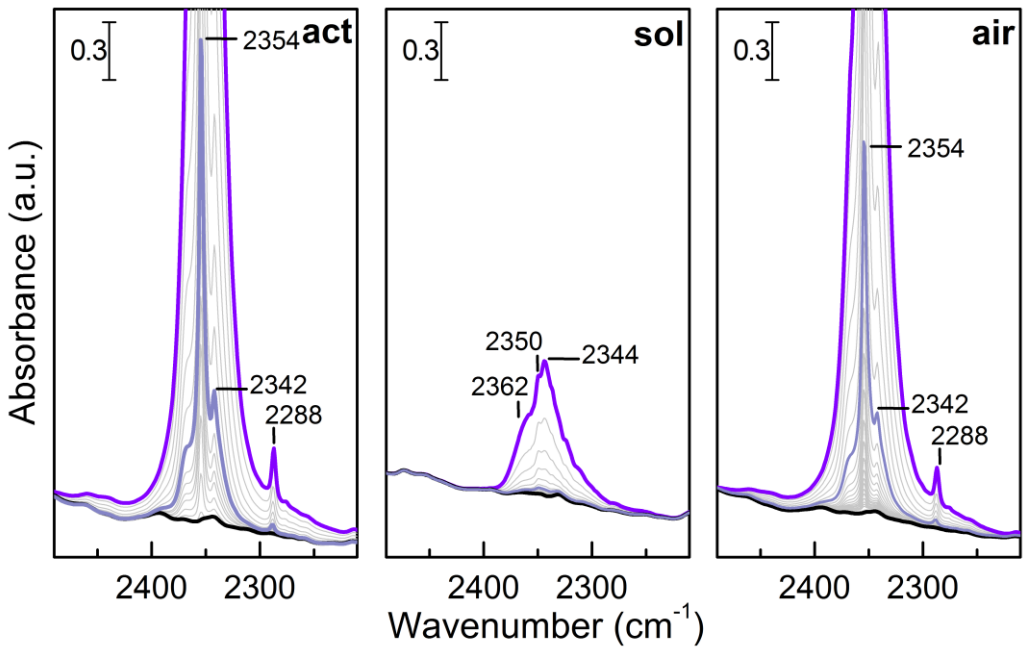

Figure 2. FTIR spectra of CO_2 adsorbed on (from left to right) Mg_2(dobpdc)–*act*, Mg_2(dobpdc)–*sol* and Mg_2(dobpdc)–*air* recorded at beam temperature. The spectra were obtained at increasing CO_2 equilibrium pressure from vacuum (black curve) to 1 mbar (light violet) and 44 mbar (violet

curve). Light grey curves refer to intermediate coverage. The spectrum obtained after prolonged degassing at beam temperature was coincident with the spectrum recorded initially in vacuum and then it was not reported. a.u. = absorbance units.

If Mg^{2+} ions are pre-coordinating a molecule with higher binding energy than CO_2, like methanol, the signals related to $CO_2 \cdots Mg^{2+}$ complexes are not expected in the spectrum. Actually, the spectrum of CO_2 on Mg_2(dobpdc)–*sol* (middle part of Figure 2) shows a significant decrease in the intensity of the CO_2 signals. This impressive decrease in CO_2 uptake is confirmed by volumetric measurements as reported in Figure S9b: at 44 mbar the uptake of –*sol* sample is only 0.1 mol kg^{-1} versus 3.1 mol kg^{-1} adsorbed by –*act*. Considering that we observe that the surface area of the –*sol* sample is approximately half of that of the –*act* sample (see Figure S9a and Table S3), we associate this 30-fold decrease of capacity to the deactivation of the major Mg^{2+} binding sites by methanol. In this case the main CO_2 band is shifted to 2344 cm^{-1}. This frequency is quite close to that recently reported for competitive adsorption of CO_2 and H_2O in IRMOF-74-I-Mg (2343 cm^{-1}, see Table 1).[4] In this article the shift was associated with the adsorption of CO_2 on a secondary site of the MOF structure, namely the linker, by establishing a hydrogen bond with the H_2O adsorbed on Mg^{2+}. A decrease of the CO_2 calculated binding energy from 41 to 38 kJ mol^{-1} was also reported upon Mg^{2+} capping.[4] Another possible description of the process can be with the adsorption of CO_2 on the pre-adsorbed methanol, that can constitute an alternative less active adsorption site in the larger pores of Mg_2(dobpdc). The lower affinity for CO_2 of the Mg^{2+} capped with methanol is also confirmed by the smaller slope of the CO_2 isotherm in the –*sol* than in the –*act* sample (see Figure S9b).[19]

Table 2. Calculated and experimental energetic, structural and vibrational features of CO_2, CO and N_2 complexes with MOF-74-Mg (from Ref. 9) and Mg_2(dobpdc) (this work) at low coverage (1:1 ratio among adsorbate molecules and Mg^{2+} sites).[a]

	Mg_2(dobpdc) *–act*							MOF-74-Mg[b]						
	ΔE^C (BSSE)	ΔE_{disp}	Δd[c]	θ[d] (Mg-O-X)	$\Delta\tilde{\nu}_{theo}$[e]	$\Delta\tilde{\nu}_{exptl}$[f]	ΔV_{cell} (%)	ΔE^C (BSSE)	ΔE_{disp}	ΔH_{exptl}	Δd[c]	θ[d] (Mg-O-X)	$\Delta\tilde{\nu}_{theo}$[e]	$\Delta\tilde{\nu}_{exptl}$[f]	ΔV_{cell} (%)
CO_2	-42.6 (4.3)	-25.7	-0.009/ 0.008	124.1/124.2	0/6/17/18	4/16	-1.3	-41.5 (4.7)	-23.2	-47	0.005/-0.007	129	10-15	15	+1.1
CO	-35.1 (4.2)	-18.5	-0.005	177.3	46-47	47	+0.2	-34.3 (4.4)	-18.1	-29	0.005	178	36-37	43	+1.1
N_2	-28.7 (5.4)	-19.3	-0.002	178.2	23-25	20	+0.1	-27.1 (6.2)	-19.0	-21	0.002	175	25	18	+1.0

[a]All the energies are reported in kJ mol^{-1}. All the frequencies are reported in cm^{-1}. [b]Data from Ref. 9. [c]Δd is the change in the bond length of the adsorbate after coordination (Å). For CO_2, the Δd relative to the C=O bond closer to Mg^{2+} is reported first. [d]θ is the angle between Mg and the two closest atoms of the adsorbate (°). [e]Calculated with respect of the value optimized for a single molecule in the gas phase (CO_2 = 2416 cm^{-1}, CO = 2219 cm^{-1}, N_2 = 2460 cm^{-1}). [f]Calculated considering as reference value that reported for adsorption in silicalite, see Table 1.

The effect of material defectivity on the CO_2 spectra was also studied by means of the Mg_2(dobpdc)*–air* sample (see right part of Figure 2). The spectra of the *–act* and *–air* samples are almost indistinguishable, indicating that also in the damaged sample the adsorption sites are the same open Mg^{2+} of the pristine material. The only effect of damaging was a decrease of 30% in the intensity of the main band (as measured at 1 mbar). Volumetric measurements allowed to

more precisely quantify the decrease in CO_2 uptake to 40% (that is very close to the qualitative estimate get from IR), that is decidedly lower than what expected from the drastic decrease in surface area (83%, see Table S3). This discrepancy was previously discussed in Ref. 5 and related to the fact that in these pressure and temperature conditions, where the main sites for CO_2 adsorption are the open metal sites, partial structural collapse leaving some of the Mg^{2+} sites available, does not qualitatively influence the gas uptake mechanism.

CO adsorption. Among the probe molecules used in this study, CO is the one experiencing the largest frequency shifts, then allowing a larger differentiation among the surface species. For this reason it is often used as probe molecule of cationic surface sites.[9] Figure 3 shows FTIR spectra of CO adsorbed on the *–act*, *–sol* and *–air* samples in the region characteristic of the CO stretching frequency (2250-2020 cm^{-1}). The whole spectral region is reported in Figure S11 in the Supporting Information. All the considerations made for CO_2 adsorption holds qualitatively also for CO.

For what concerns Mg_2(dobpdc)*–act* and Mg_2(dobpdc)*–air*, CO adsorption is already observed at beam temperature as expected on the basis of the calculated adsorption energy for 1:1 CO/Mg^{2+} complexes (35.1 kJ mol^{-1}, see Table 2) and similarly to what reported for MOF-74-Mg.[9] As already observed for CO_2, a slightly higher CO shift was measured in Mg_2(dobpdc) with respect to MOF-74-Mg, a result also validated by the calculations (see Table 1 and Table 2). No CO signal is observed at RT for Mg_2(dobpdc)*–sol* (Figure **3**-*sol*, inset), proving the efficient capping action by methanol molecules of Mg^{2+} sites. For the *–air* sample, the CO frequency was the same observed for act, but decreased in intensity of about 30%.

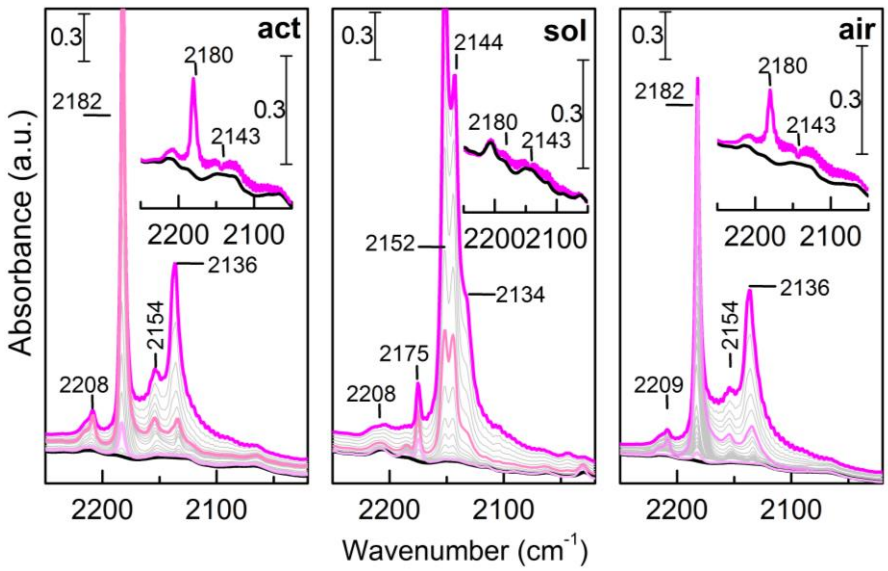

Figure 3. FTIR spectra recorded at 100 K of CO adsorbed on (from left to right) Mg_2(dobpdc)–*act*, Mg_2(dobpdc)–*sol* and Mg_2(dobpdc)–*air*. 44 mbar of CO were dosed at beam temperature on the sample (spectra reported in the insets) and then the temperature was decreased to 100 K (spectra not shown). Once that equilibrium was reached, the spectra were recorded upon decreasing CO equilibrium pressure from 12 mbar (pink curve) to vacuum (black curve). Spectra recorded at 1 and 0.01 mbar equilibrium pressures have been indicated with pink shades. Light grey curves refer to intermediate coverage. The spectrum obtained after prolonged degassing at >100 K was coincident with the spectrum recorded initially in vacuum and then it was not reported. a.u. = absorbance units.

The normal liquefaction temperature of CO is 81.6 K. Because of that IR studies at 100 K are very common: temperature decrease causes an increase in the CO coverage and because of the

proximity to the CO boiling point, an adsorbed liquid like phase is formed. In these conditions, the interaction of CO with the whole material surface is reached also at sub-atmospheric pressures, permitting the characterization of all the adsorption sites.

Lowering the temperature to about 100 K caused the appearance of a complex family of bands on all the samples in the CO stretching region (dark pink curves). These bands are gradually removed upon decreasing the pressure. For the sake of clarity, in the following the CO spectra at 100 K will be described as if they were obtained by increasing the CO pressure.

Also at 100 K, the *–air* spectra showed a similar behavior to the *–act* ones, besides the lower intensity of the IR signals in the damaged sample. At lower coverage, the spectrum of Mg_2(dobpdc)*–act* is characterized by a single band, slightly blueshifted with respect to the BT value (2182 versus 2180 cm^{-1}). This band remains the most intense also at the highest pressure considered here (12 mbar), slightly redshifting with coverage because of the progressive increase of the dipole-dipole coupling among the oscillators. This band is missing in the Mg_2(dobpdc)*–sol* spectra, being substituted by a weak and sharp signal at 2175 cm^{-1}.

Upon increasing the pressure, other bands appeared at 2154 and 2134 cm^{-1} in all the samples, that can be associated to CO interaction with the MOF linker and to liquid like-CO filling the MOF pores, respectively.[43] Nevertheless, the intensity of the band at 2154 cm^{-1} was found to be strongly dependent on the quality of the activation of the sample and it starts to appear in the Mg_2(dobpdc)*–act* spectrum only simultaneously to liquid like-CO band. It is also the most intense band in the Mg_2(dobpdc)*–sol* spectrum, although slightly shifted (2152 cm^{-1}). Moreover, a shift of +17 cm^{-1} cannot be associated to the interaction of CO with apolar species as biphenyl. The 2154 cm^{-1} signal is then more likely associated to the interaction of CO with molecules

preadsorbed on Mg^{2+} sites as solvent molecules or other CO molecules. Therefore, the intensity of the 2154 cm^{-1} band can be used to check the quality of activation procedures or the homogeneity of the grafting of molecules on Mg^{2+} sites. A signal at 2154 cm^{-1} was absent in MOF-74-Mg likely because of its smaller pore dimension, not allowing CO adsorption on top of preexisting CO/Mg^{2+} complexes. Besides the signal at 2152 cm^{-1}, the *–sol* spectra are dominated by an additional band at 2144 cm^{-1}. The 2152 and 2144 cm^{-1} bands appeared and growth in parallel, suggesting their association to species characterized by a similar binding, as for example CO in interaction with methanol molecules in two different configurations.

In all the samples, a very weak band was observed at about 2210 cm^{-1}. This band has been previously reported for CO adsorption on oxide defects.[43] Nevertheless, at least in this case it is more likely associated to a modification of the framework modes due to adsorption, being also observed upon N_2 adsorption (see Figure S13). This is not the only framework mode perturbed by gas adsorption, as visible in the insets of Figure S11act. In these spectra, the appearance of signals in the 3800-3600 cm^{-1} region upon N_2 dosing is noteworthy. These bands can be assigned to overtones of the bands at about 1900-1800 cm^{-1}, that are strongly modified upon adsorption. The assignment of those features to water impurities in the gas can be ruled out, being them completely removed upon degassing also at 77 K, unlike those of water that can be removed only upon heating at $T > 180°C$. These signals were also observed for N_2 adsorption, their intensity growing with the coverage and with the binding energy of the adsorbate. In the case of CO_2 the signals at 3800-3600 cm^{-1} were covered by the intense CO_2 Fermi resonance bands and for this reason they were not detected (see Figure S10act).

N_2 adsorption. The IR-inactive N_2 probe-molecule becomes active only when polarized by strong binding sites. For this reason, it gives rise to simpler spectra which are usually easier to assign. Strongly perturbing sites are for example the open Mg^{2+} sites of Mg_2(dobpdc). Infrared spectra of N_2 adsorbed on the *-act, –sol* and *–air* Mg_2(dobpdc) materials are reported in Figure 4 in the N_2 stretching frequency region (2400-2300 cm^{-1}). The whole spectral region is reported in Figure S12. The spectrum of Mg_2(dobpdc)*–act* is characterized by a single peak at 2341 cm^{-1} at BT, assigned to the adsorption on Mg^{2+} sites on the basis of previous literature data[9] and of the calculations (see Table 2). All the considerations made for CO adsorption hold also for N_2. Also in this case, the only difference between *–act* and *–air* spectra was the intensity of the N_2 band, that is 61% for *–air* with respect to act. The absence of any signal related to N_2 in the spectrum recorded for Mg_2(dobpdc)*–sol* is impressive (middle part of Figure 4). Unlike what done for CO_2, in this case the quantification of the Mg^{2+} sites by means of nitrogen volumetric measurements at 77 K was unsuccessful (isotherms reported in Figure S9a).[5] In fact, unlike in the IR experiment, that is sensitive only to adsorbed N_2 molecules on open metal sites, in the volumetric measurements all the N_2 molecules (both IR–*act*ive or inactive) are "counted".

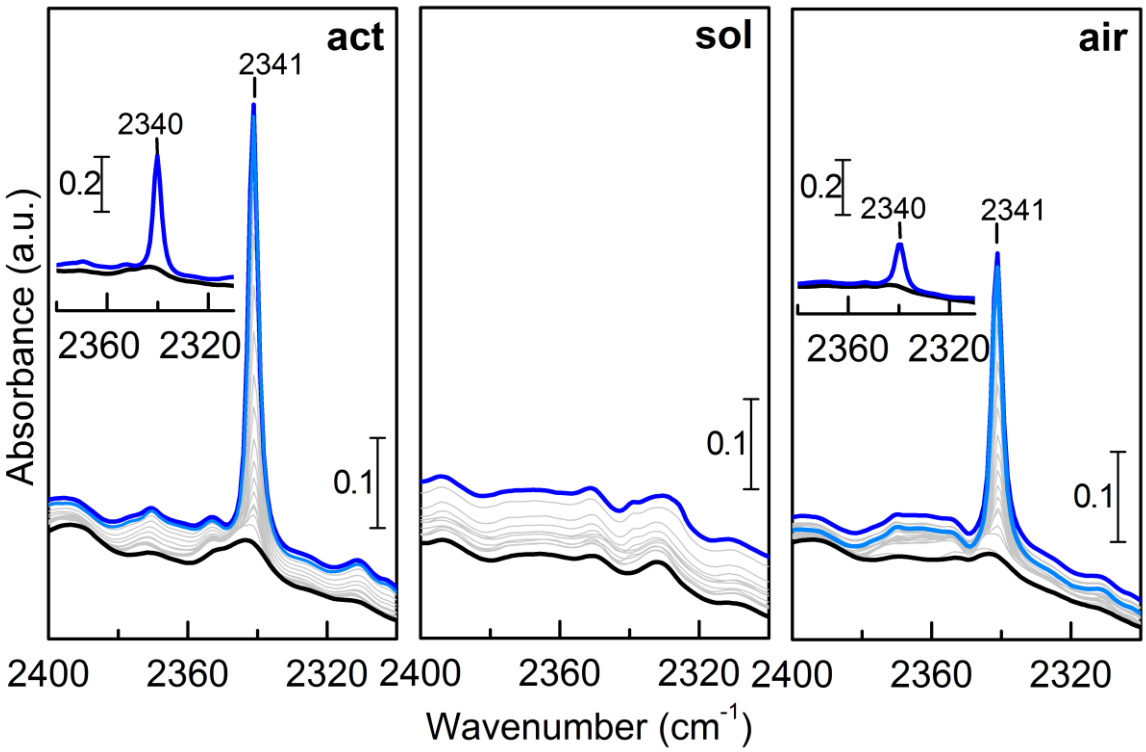

Figure 4. FTIR spectra of N_2 at 100 K adsorbed on (from left to right) Mg_2(dobpdc)–*act*, Mg_2(dobpdc)–*sol* and Mg_2(dobpdc)–*air*. 44 mbar of N_2 were dosed at beam temperature on the sample (spectra reported in the insets) and then the temperature was decreased to approximately 100 K. Once equilibrium was reached, the spectra were recorded upon decreasing N_2 equilibrium pressure from 41 mbar (blue curve) to vacuum (black curve). Light grey curves refer to intermediate coverage besides the one recorded at 21 mbar that is marked with a light blue curve. The spectrum obtained after prolonged degassing at T >100 K was coincident with the spectrum recorded initially in vacuum and then it was not reported. a.u. = absorbance units.

Upon lowering the temperature to 100 K, no additional bands related to N_2 appeared in the spectra, not only for Mg_2(dobpdc)–*act* and –*air* but also for Mg_2(dobpdc)–*sol*, allowing to better

appreciate the framework perturbations (see 3800-3540 and 1975-1810 cm^{-1} spectral regions in Figure S12 in the Supporting information).

Discussions

Effect of pore size. By analyzing the data reported in Table 1 and Table 2 or by considering Figure 5 and Figure 6, a larger affinity between the MOF and the guests is observed for Mg_2(dobpdc) with respect to MOF-74-Mg, that is for the material with the larger pore size. This can be regarded as an anomaly in the IRMOF-70 family, where adsorption enthalphy is expected to decrease with increasing pore size. On the other hand, Mg_2(dobpdc) does not contain specific adsorption sites other than those present in both the smaller and larger members of the family. Therefore, its anomalous high affinity for adsorbated is expected to result from a fine balance among structural features favouring adsorption. The analysis of the structural changes and of the different energetic components to the interaction allowed to evidence two origins of this result.

Both qualitative expectations and previous cluster calculations[44] showed that the superposition of the electrostatic potential from two opposite walls in a material pore fades quickly with increasing pore dimension. In this case, the pore size is increased by 7 Å a significant amount for this kind of phenomenon. On the contrary, in this case the dispersion contribution to the interaction ($|\Delta E_{disp}|$) slightly increases with the pore dimension for all the adsorbates (see Figure 6) likely because of the increased number of atoms giving a not negligible contribution to ΔE_{disp} per molecule of adsorbate. It is in fact important to notice that more than the 50% of the adsorption energy is accounted to the dispersion energy (see Table 2 and Figure 6), in agreement with previous reports.[8-9] The important role of dispersion forces is evident if the adsorption

enthalpy of CO on the open MgO(001) surface (-13 kJ mol^{-1})[9] is compared to that obtained for Mg_2(dobpdc) (-29 kJ mol^{-1}). Secondly, the deformation necessary to the framework to accommodate the guest molecules in the material is lower for the MOF with larger pores (compare ΔV% in Table 2). The only exception is observed for CO_2 where the ΔV% are comparable in modulus but opposite in sign. Nevertheless, as discussed above, in this case the shrinking of the Mg_2(dobpdc) volume causes a further increase in the dispersion energy of about 2 kJ mol^{-1} with respect to that calculated for the complex in an almost unvaried cell (ΔV% = 0.0), that is it allows a greater stabilization of the CO_2 complex. For what concerns the hypothesis of a higher polarity of the Mg_2(dobpdc) framework and especially of the Mg^{2+} site, it was ruled out by the comparison of the Mulliken charges (+1.45 and +1.44 for Mg_2(dobpdc) and MOF-74-Mg, respectively) and of the electrostatic potential maps (see Figure S15) essentially identical for the two structures.

eIt has been reported by several authors that $\Delta\tilde{\nu}_{CO}$ is directy related to ΔH_{CO} (see for example Ref. 9). Accordingly, larger $\Delta\tilde{\nu}$ for all the molecular probes are observed both experimentally (see Figure 6) and theoretically (see Table 2) for the complexes in the MOF with the larger pores because of the larger affinity. The calculated shifts are in very good agreement with those obtained experimentally, further validating the models adopted.

Among the three adsorbates considered in this study, dinitrogen is the one showing the highest increase in $|\Delta E|$ upon increasing the pore size both on absolute (1.6 versus 1.1 and 0.8 kJ mol^{-1} for N_2, CO_2 and CO, respectively) and relative terms (6% for N_2 versus 3% for CO_2 and 2% for CO). This allows to predict a lower selectivity factor for the separation for CO_2 and N_2 in a gas

stream for Mg_2(dobpdc) with respect to MOF-74-Mg, although the adsorption site structures would suggest very similar performances for the two materials.

For what concerns the comparison of IR spectroscopic features, whereas CO_2 and N_2 undergo a slight increase in the $\Delta\tilde{\nu}$ associated to the molecules in direct interaction with a Mg^{2+} site in Mg_2(dobpdc) with respect to MOF-74-Mg (about 1-2 cm^{-1}), in the case of CO an increase of 4 cm^{-1} is observed. In relative terms, it is N_2, with an 11% increase of $\Delta\tilde{\nu}$, the molecular probe showing the largest difference when adsorbed on the two materials.

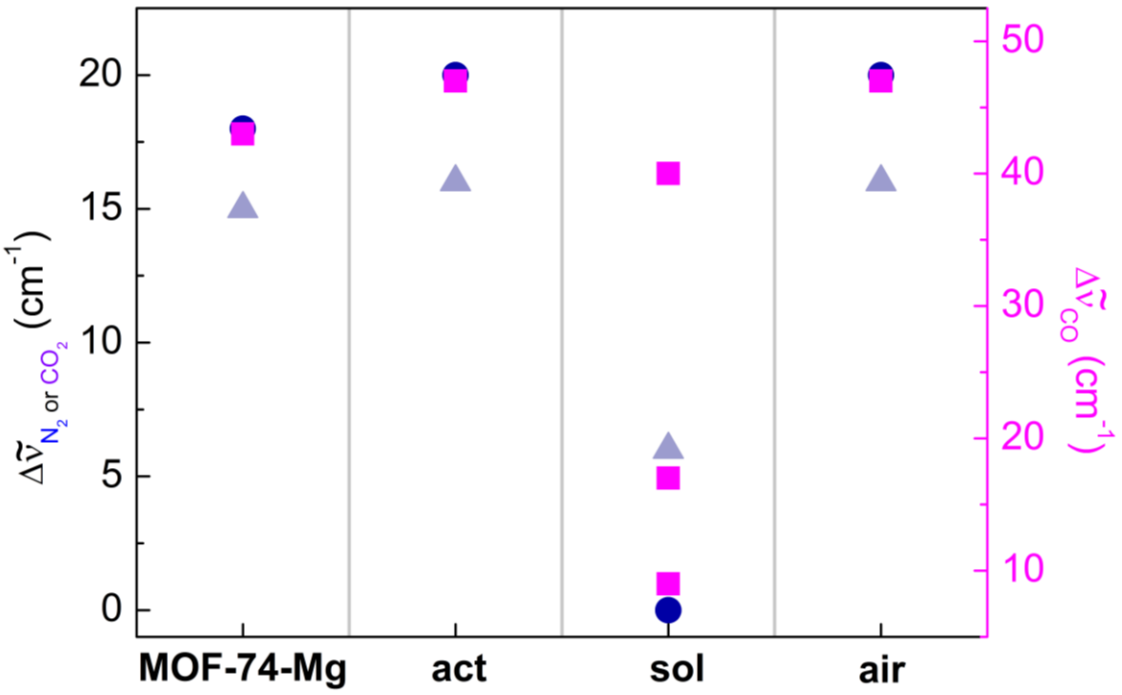

Figure 5. Frequency shift of CO_2 (violet triangles), CO (magenta squares) and N_2 (blue circles) after adsorption on MOF-74-Mg,[9] Mg_2(dobpdc)–*act*, Mg_2(dobpdc)–*sol* and Mg_2(dobpdc)–*air* at

low coverage (value reported in Table **1**,reference frequency in silicalite-1 = 21XX cm^{-1}). The drastic effect of metal site poisoning by preadsorbed solvent molecules on the perturbation of CO_2, CO and N_2 is evident.

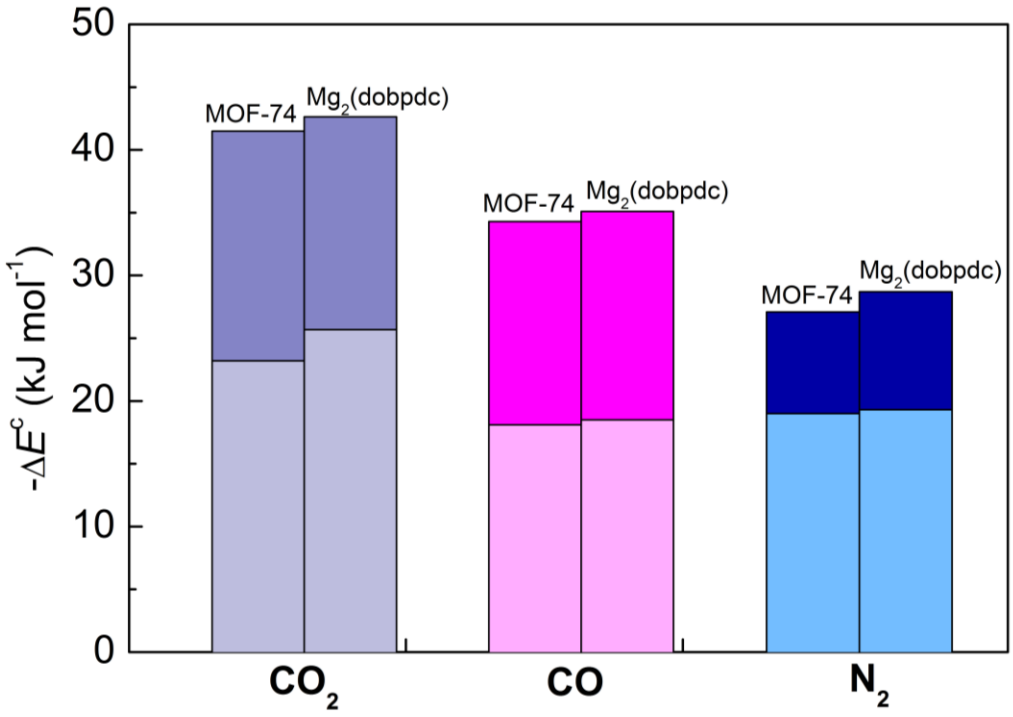

Figure 6. Computed total adsorption energy (entire bar height) and dispersion energy contribution (lighter colors) for the interaction of CO_2 (violet), CO (magenta) and N_2 (blue) with MOF-74-Mg (values from Ref. 9) and Mg_2(dobpdc)–*act* (this work) as obtained at the B3LYP-D*/TZVp level of theory.

Effect of defects and material damage. The effect of damaging is not clearly detectable by substantial changes in the infrared spectra of both the MOF and the guests. This is well evident

comparing the data for the *–act* and the *–air* sample in Figure 6 and in Table 1. Extensive structural collapse (decrease of 83% in the Langmuir surface area) caused only a 30-40% decrease in the intensity of all the bands relative to the adsorbates for all the molecular probes considered but it did not change the qualitative appearance of the spectra. This was verified not only for CO_2 and N_2 that are showing, for different reasons, only the features associated with Mg^{2+} sites, but also for CO which is able to probe different parts of the MOF structure. This means that the MOF degradation by hydrolysis does not induce the formation of new phases and a high degree of short range order is maintained in the damaged material. This is likely due to the combination of an overall robustness of the lattice, accompanied by a certain flexibility of the ligands. Please refer to Ref. 5 for a more extensive discussion on this point.

Effect of solvation. Open magnesium sites represent by far the strongest adsorption sites in both Mg_2(dobpdc) and MOF-74-Mg, whereas the largest part of the MOF surface is almost apolar, being constituted by phenyl rings. The drastic change observed in the IR spectrum of all the molecular probes upon Mg^{2+} poisoning was therefore expected. N_2 was the most affected probe, showing no IR signals also at 100 K, although an uptake equal to the 50% of that measured for Mg_2(dobpdc)*–act* was verified by volumetric measurements (see Figure S9a). Nevertheless, all these N_2 molecules remain invisible by IR spectroscopy being only slightly perturbed by the nanoscaffold. Also in the case of CO_2, besides the expected disappearance of the features associated to CO_2 ··Mg^{2+} species, a drastic reduction of the peak intensity was verified, larger than the 50% reduction in surface area (see Table S3). Accordingly, a strong decrease in CO_2 uptake was verified by volumetric measurements, quantifying the CO_2 adsorbed by *–sol* to only 1% of the amount get by -*act*. This result indicates that the apolar nanoscaffold is not able to

significantly bound CO_2. Moreover, also the solvent molecules in direct interaction with Mg^{2+} are not sufficiently polarized to constitute a strong adsorption site for CO_2 (and N_2). Similarly CO at BT shows only the gas phase signals in sol. On the contrary, at 100 K, CO showed a significant and complex family of bands. Among these bands, the relative intensity of the signal at 2154 cm^{-1} was found to be significantly influenced by the presence of molecules of any nature preadsorbed on the Mg^{2+} sites (solvent, CO itself, …). A band at 2144 cm^{-1} was observed only in CO/Mg_2(dobpdc)–*sol*. This band is not present in partially activated Mg_2(dobpdc) samples prepared *ad hoc* . It is specific of the -*sol* system and therefore it is not a suggested marker for quality check purposes.

Conclusions

Metal-organic frameworks (MOFs) are hybrid organic-inorganic materials that have showed superior performances with respect to all the other classes of materials in a large variety of sorptive applications. Adsorption properties of engineered MOFs critically depend on a variety of factors, including pore size and flexibility, the availability of open metal sites and the presence of defect sites. Mg_2(dobpdc) is one of the most important MOFs, because of its unique performances in carbon dioxide capture and storage technologies when combined with aliphatic amines. We have adopted this material as a paradigmatic case for the study of the above mentioned factors on sorptive properties. In this study several molecular probes (CO_2, CO, N_2) have been adopted in order to characterize the adsorption sites in the material. Several solvents (H_2O, CH_2Cl_2, CH_3OH, toluene) have been adsorbed on the MOF from the gas phase and the reversibility of the adsorption at beam temperature has been tested. Toluene and CH_2Cl_2

adsorption was found to be fully reversible upon degassing at beam temperature. Therefore, they can then be indicated as suitable dispersing agents for weakly binding guest molecules in the Mg_2(dobpdc) pores or for formulation and shaping processes. On the contrary, methanol was verified to be a good capping agent for the Mg^{2+} sites being strongly and irreversibly bound at beam temperature, without causing hydrolysis of the material. It was therefore adopted as capping agent for the study of adsorption of CO_2, CO and N_2 on sites other than uncoordinated Mg^{2+}. In particular, the CO band at 2154 cm^{-1} was identified as due to the interaction of CO with pre-adsorbed molecules on Mg^{2+}. This band can then be used to quickly test the quality of an activation procedure. Adsorption at RT-40°C, especially of CO and N_2, being essentially driven by open Mg^{2+} sites, can be exploited for easy and effective quality testing of amine/MOF composites synthesis, evidencing the presence of unsaturated Mg^{2+}. Because of the air-sensitivity of Mg_2(dobpdc), a full IR characterization was also performed after exposing the MOF to a saturated water atmosphere overnight followed by reactivation. Surprisingly, besides a decrease in the intensity of the probe molecules bands, suggesting a slightly lower uptake, no difference was observed in the spectra with respect to the pristine material, despite a significant structural loss (83% surface area). FTIR spectroscopy of probe molecules does not represent then a reliable technique to detect material damaging in MOF materials. Nevertheless, this result also suggests that Mg_2(dobpdc) maintains almost unvaried its CO_2/N_2/CO separation performances also after extensive material decomposition.

ASSOCIATED CONTENT

Supporting Information. Optimised structures of Mg_2(dobpdc)–*act*, CO_2/Mg_2(dobpdc)–*act*, CO/Mg_2(dobpdc)–*act* and N_2/Mg_2(dobpdc)–*act*; ATR-FTIR spectrum of Mg_2(dobpdc)–*act*, calculated IR spectrum of Mg_2(dobpdc)–*act*; IR spectra of toluene, chloroform, methanol, and water on Mg_2(dobpdc)–*act*, Volumetric measurements of N_2 at 77 K and CO_2 at RT; IR spectra of CO_2, CO and N_2 on Mg_2(dobpdc)–*act*, on Mg_2(dobpdc)–*sol* and Mg_2(dobpdc)–*air*; Calculated vibrational modes of Mg_2(dobpdc)–*act*, CO_2/Mg_2(dobpdc)–*act*, CO/Mg_2(dobpdc)–*act* and N_2/Mg_2(dobpdc)–*act*. This material is available free of charge via the Internet at http://pubs.acs.org.

AUTHOR INFORMATION

Corresponding Author

*Department of Chemistry, University of Minnesota, 207 Pleasant Street S.E., Minneapolis, MN 55455-0431. Phone: 612-624-5923. E-mail: jg.vitillo@gmail.com.

Author Contributions

All authors have given approval to the final version of the manuscript.

ACKNOWLEDGMENTS

Prof. Bartolomeo Civalleri and Prof. Silvia Bordiga are strongly acknowledged for discussion and help with the periodic calculations.

ABBREVIATIONS

MOFs, metal organic frameworks; FTIR, Fourier-transformed infrared; BT, beam temperature; H_4-dobpdc = 4,4'-dihydroxy-(1,1'-biphenyl)-3,3'-dicarboxylic acid.

REFERENCES

(1) Silva, P.; Vilela, S. M. F.; Tome, J. P. C.; Almeida Paz, F. A. *Multifunctional metal-organic frameworks: from academia to industrial applications*, *Chem. Soc. Rev.* **2015**, *44*, 6774.
(2) Furukawa, H.; Cordova, K. E.; O'Keeffe, M.; Yaghi, O. M. *The Chemistry and Applications of Metal-Organic Frameworks*, *Science* **2013**, *341*.
(3) Tan, K.; Zuluaga, S.; Gong, Q.; Canepa, P.; Wang, H.; Li, J.; Chabal, Y. J.; Thonhauser, T. *Water Reaction Mechanism in Metal Organic Frameworks with Coordinatively Unsaturated Metal Ions: MOF-74*, *Chem. Mater.* **2014**, *26*, 6886.
(4) Tan, K.; Zuluaga, S.; Gong, Q.; Gao, Y.; Nijem, N.; Li, J.; Thonhauser, T.; Chabal, Y. J. *Competitive Coadsorption of CO_2 with H_2O, NH_3, SO_2, NO, NO_2, N_2, O_2, and CH_4 in M-MOF-74 (M = Mg, Co, Ni): The Role of Hydrogen Bonding*, *Chem. Mater.* **2015**, *27*, 2203.
(5) Vitillo, J. G.; Bordiga, S. *Increasing the stability of Mg_2(dobpdc) metal-organic framework in air through solvent removal*, *Mater. Chem. Front.* **2017**, *1*, 444.
(6) Sumida, K.; Rogow, D. L.; Mason, J. A.; McDonald, T. M.; Bloch, E. D.; Herm, Z. R.; Bae, T. H.; Long, J. R. *Carbon Dioxide Capture in Metal-Organic Frameworks*, *Chem. Rev.* **2012**, *112*, 724.
(7) Gygi, D.; Bloch, E. D.; Mason, J. A.; Hudson, M. R.; Gonzalez, M. I.; Siegelman, R. L.; Darwish, T. A.; Queen, W. L.; Brown, C. M.; Long, J. R. *Hydrogen Storage in the Expanded Pore Metal-Organic Frameworks M_2(dobpdc) (M = Mg, Mn, Fe, Co, Ni, Zn)*, *Chem. Mater.* **2016**, *28*, 1128.
(8) Lee, K.; Howe, J. D.; Lin, L.-C.; Smit, B.; Neaton, J. B. *Small-Molecule Adsorption in Open-Site Metal–Organic Frameworks: A Systematic Density Functional Theory Study for Rational Design*, *Chem. Mater.* **2015**, *27*, 668.
(9) Valenzano, L.; Civalleri, B.; Chavan, S.; Turnes Palomino, G.; Otero Areán, C.; Bordiga, S. *Computational and Experimental Studies on the Adsorption of CO, N_2, and CO_2 on Mg-MOF-74*, *J. Phys. Chem. C* **2010**, *114*, 11185.
(10) Vitillo, J. G. *Magnesium-Based Systems for Carbon Dioxide Capture, Storage and Recycling: from Leaves to Synthetic Nanostructured Materials*, *RSC Adv.* **2015**, *5*, 36192.
(11) Masala, A.; Vitillo, J. G.; Mondino, G.; Grande, C. A.; Blom, R.; Manzoli, M.; Marshall, M.; Bordiga, S. *CO_2 Capture in Dry and Wet Conditions in UTSA-16 Metal–Organic Framework*, *ACS Appl. Mater. Interf.* **2017**, *9*, 455.
(12) McDonald, T. M.; Mason, J. A.; Kong, X.; Bloch, E. D.; Gygi, D.; Dani, A.; Crocella, V.; Giordanino, F.; Odoh, S. O.; Drisdell, W. S.; Vlaisavljevich, B.; Dzubak, A. L.; Poloni, R.; Schnell, S. K.; Planas, N.; Lee, K.; Pascal, T.; Wan, L. F.; Prendergast, D.; Neaton, J. B.; Smit, B.; Kortright, J. B.; Gagliardi, L.; Bordiga, S.; Reimer, J. A.; Long, J. R. *Cooperative Insertion of CO_2 in Diamine-Appended Metal-Organic Frameworks*, *Nature* **2015**, *519*, 303.
(13) Lee, W. R.; Jo, H.; Yang, L.-M.; Lee, H.; Ryu, D. W.; Lim, K. S.; Song, J. H.; Min, D. Y.; Han, S. S.; Seo, J. G.; Park, Y. K.; Moon, D.; Hong, C. S. *Exceptional CO_2 Working Capacity in a Heterodiamine-Grafted Metal-Organic Framework*, *Chem. Sci.* **2015**, *6*, 3697.
(14) Grimme, S. *Semiempirical GGA-type density functional constructed with a long-range dispersion correction*, *J. Comput. Chem.* **2006**, *27*, 1787.

(15) Civalleri, B.; Zicovich-Wilson, C. M.; Valenzano, L.; Ugliengo, P. *B3LYP augmented with an empirical dispersion term (B3LYP-D*) as applied to molecular crystals*, *Cryst. Eng. Comm.* **2008**, *10*, 405.
(16) Ethiraj, J.; Albanese, E.; Civalleri, B.; Vitillo, J. G.; Bonino, F.; Chavan, S.; Shearer, G. C.; Lillerud, K. P.; Bordiga, S. *Carbon Dioxide Adsorption in Amine-Functionalized Mixed-Ligand Metal–Organic Frameworks of UiO-66 Topology*, *Chem. Sus. Chem.* **2014**, *7*, 3382.
(17) Caskey, S. R.; Wong-Foy, A. G.; Matzger, A. J. *Dramatic Tuning of Carbon Dioxide Uptake via Metal Substitution in a Coordination Polymer with Cylindrical Pores*, *J. Am. Chem. Soc.* **2008**, *130*, 10870.
(18) Leclerc, H.; Vimont, A.; Lavalley, J.-C.; Daturi, M.; Wiersum, A. D.; Llwellyn, P. L.; Horcajada, P.; Ferey, G.; Serre, C. *Infrared study of the influence of reducible iron(iii) metal sites on the adsorption of CO, CO2, propane, propene and propyne in the mesoporous metal-organic framework MIL-100*, *Phys. Chem. Chem. Phys.* **2011**, *13*, 11748.
(19) Gregg, S. J.; Sing, K. S. W. *Adsorption, surface area and porosity (2nd ed.)*; Academic Press Inc.: London, 1982.
(20) Langmuir, I. *The Adsorption of Gases on Plane Surfaces of Glass, Mica and Platinum*, *J. Am. Chem. Soc.* **1918**, *40*, 1361.
(21) Dovesi, R.; Orlando, R.; Erba, A.; Zicovich-Wilson, C. M.; Civalleri, B.; Casassa, S.; Maschio, L.; Ferrabone, M.; De La Pierre, M.; D'Arco, P.; Noel, Y.; Causa, M.; Rerat, M.; Kirtman, B. *CRYSTAL14: A Program for the Ab Initio Investigation of Crystalline Solids*, *Int. J. Quantum Chem.* **2014**, *114*, 1287.
(22) Becke, A. D. *Density-Functional Thermochemistry 3. The Role of Exact Exchange*, *J. Chem. Phys.* **1993**, *98*, 5648.
(23) Lee, C.; Yang, W.; Parr, R. G. *Development of the Colle-Salvetti correlation-energy formula into a functional of the electron density*, *Phys. Rev. B* **1988**, *37*, 785.
(24) Song, Q.; Nataraj, S. K.; Roussenova, M. V.; Tan, J. C.; Hughes, D. J.; Li, W.; Bourgoin, P.; Alam, M. A.; Cheetham, A. K.; Al-Muhtaseb, S. A.; Sivaniah, E. *Zeolitic imidazolate framework (ZIF-8) based polymer nanocomposite membranes for gas separation*, *Energy Environ. Sci.* **2012**, *5*, 8359.
(25) Broyden, C. G. *A class of methods for solving nonlinear simultaneous equations*, *Math. Comput.* **1965**, *19*, 577.
(26) Johnson, D. D. *Modified Broyden's method for accelerating convergence in self-consistent calculations*, *Phys. Rev. B* **1988**, *38*, 12807.
(27) Lendvay, G.; Mayer, I. *Some difficulties in computing BSSE-corrected potential surfaces of chemical reactions*, *Chem Phys Lett* **1998**, *297*, 365.
(28) Pascale, F.; Zicovich-Wilson, C. M.; López Gejo, F.; Civalleri, B.; Orlando, R.; Dovesi, R. *The calculation of the vibrational frequencies of crystalline compounds and its implementation in the CRYSTAL code*, *J. Comput. Chem.* **2004**, *25*, 888.
(29) Bonino, F.; Lamberti, C.; Chavan, S.; Vitillo, J. G.; Bordiga, S. In *Metal Organic Frameworks as Heterogeneous Catalysts*; Llabrés i Xamena, F., Gascon, J., Eds.; RSC Catalysis Series: Cambridge, 2013.
(30) Chavan, S. M.; Shearer, G. C.; Svelle, S.; Olsbye, U.; Bonino, F.; Ethiraj, J.; Lillerud, K. P.; Bordiga, S. *Synthesis and Characterization of Amine-Functionalized Mixed-Ligand Metal–Organic Frameworks of UiO-66 Topology*, *Inorg. Chem.* **2014**, *53*, 9509.

(31) Valenzano, L.; Vitillo, J. G.; Chavan, S.; Civalleri, B.; Bonino, F.; Bordiga, S.; Lamberti, C. *Structure-activity relationships of simple molecules adsorbed on CPO-27-Ni metal-organic framework: In situ experiments vs. theory*, *Catal. Today* **2012**, *182*, 67.
(32) Colthup, N. B.; Daly, L. H.; Wiberley, S. E. *Introduction to Infrared and Raman Spectroscopy (Third Edition)*; Academic Press: San Diego, 1990.
(33) Vitillo, J. G.; Savonnet, M.; Ricchiardi, G.; Bordiga, S. *Tailoring Metal-Organic Frameworks for CO2 Capture: The Amino Effect*, *Chem. Sus. Chem.* **2011**, *4*, 1281.
(34) Farzaneh, A.; Zhou, M.; Potapova, E.; Bacsik, Z.; Ohlin, L.; Holmgren, A.; Hedlund, J.; Grahn, M. *Adsorption of Water and Butanol in Silicalite-1 Film Studied with in Situ Attenuated Total Reflectance–Fourier Transform Infrared Spectroscopy*, *Langmuir* **2015**, *31*, 4887.
(35) FitzGerald, S. A.; Schloss, J. M.; Pierce, C. J.; Thompson, B.; Rowsell, J. L. C.; Yu, K.; Schmidt, J. R. *Insights into the Anomalous Vibrational Frequency Shifts of CO2 Adsorbed to Metal Sites in Microporous Frameworks*, *J. Phys. Chem. C* **2015**, *119*, 5293.
(36) Bonelli, B.; Civalleri, B.; Fubini, B.; Ugliengo, P.; Otero Areán, C.; Garrone, E. *Experimental and Quantum Chemical Studies on the Adsorption of Carbon Dioxide on Alkali-Metal-Exchanged ZSM-5 Zeolites*, *J. Phys. Chem. B* **2000**, *104*, 10978.
(37) Roque-Malherbe, R.; Polanco-Estrella, R.; Marquez-Linares, F. *Study of the Interaction between Silica Surfaces and the Carbon Dioxide Molecule*, *J. Phys. Chem. C* **2010**, *114*, 17773.
(38) Pulido, A.; Delgado, M. R.; Bludsky, O.; Rubes, M.; Nachtigall, P.; Arean, C. O. *Combined DFT/CC and IR spectroscopic studies on carbon dioxide adsorption on the zeolite H-FER*, *Energy Environ. Sci.* **2009**, *2*, 1187.
(39) Pirngruber, G. D.; Raybaud, P.; Belmabkhout, Y.; Cejka, J.; Zukal, A. *The role of the extra-framework cations in the adsorption of CO2 on faujasite Y*, *Phys. Chem. Chem. Phys.* **2010**, *12*, 13534.
(40) Vaidhyanathan, R.; Iremonger, S. S.; Dawson, K. W.; Shimizu, G. K. H. *An amine-functionalized metal organic framework for preferential CO2 adsorption at low pressures*, *Chem. Commun.* **2009**, 5230.
(41) Vitillo, J. G.; Ricchiardi, G.; Spoto, G.; Zecchina, A. *Theoretical maximal storage of hydrogen in zeolitic frameworks*, *Phys. Chem. Chem. Phys.* **2005**, *7*, 3948.
(42) Sarakhov, A. I.; Kononyuk, V. F.; Dubinin, M. M. In *Molecular Sieves*; American Chemical Society, 1973; Vol. 121.
(43) Zecchina, A.; Scarano, D.; Bordiga, S.; Spoto, G.; Lamberti, C. In *Advances in Catalysis*; Academic Press, 2001; Vol. Volume 46.
(44) Vitillo, J. G.; Atzori, C.; Civalleri, B.; Barbero, N.; Barolo, C.; Bonino, F. In *Hybrid organic-inorganic interfaces. Towards advanced functional materials*; Delville, M. H., Taubert, A., Eds.; Wiley-VCH Verlag, 2017.

TOC Graphic

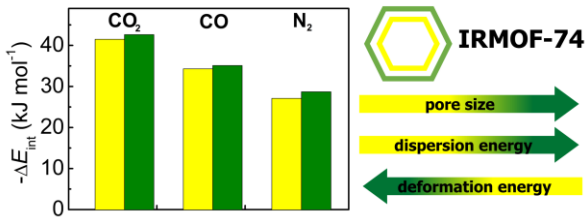
CO2
CO
N2
-ΔEint (kJ mol-1)
0
10
20
30
40
IRMOF-74
pore size
dispersion energy
deformation energy